RSC Advances

This article can be cited before page numbers have been issued, to do this please use: J. Yao, Z. zhang, Y. Zhao, W. Jing and G. Zuo, *RSC Adv.*, 2016, DOI: 10.1039/C6RA05131F.

ROYAL SOCIETY OF CHEMISTRY

www.rsc.org/advances

View Article Online
DOI: 10.1039/C6RA05131F

RSC Advances

COMMUNICATION

Title: Double-stranded probe modified AuNPs for sensitive and selective detection of microRNA 30a in solution and live cell

Received 00th January 20xx,
Accepted 00th January 20xx

DOI: 10.1039/x0xx00000x

www.rsc.org/

Juan Yao[a], Zhang Zhang[a], Yingze Zhao[b], Wanli Jing[c], Guowei Zuo[a],*

Recent advances in miRNA research have posed a new direction in biology and chemistry to uncover the complex roles of ribonucleic acids in cellular processes. A reliable sensing strategy that can monitor the miRNA expression in live cancer cells associated with bioprocesses and biomedical applications is urgently needed. Conventional miRNA sensing methods include Northern blot, microarrays and real-time quantitative PCR. However, none of them can monitor miRNA real-time expression levels in cancer cells. In this article, we reported a double-stranded DNA probe modified gold nanoparticle used as both "nano-flares" and transfection agents to quantify miR-30a in solution further visualize in live cells. This proposed strategy not only enables to quantify (in a concentration range from 5 pM to 200 pM with a detection limit of 2.4 pM) and to specifically detect miRNA levels in solution, but also allows precise and in situ monitor the changes of miRNA expression levels in live cells. The proposed method is simple and cost-effective, holding great promise for clinical applications.

1. Introduction

microRNAs (miRNAs) are small molecules ranging from 17 to 22 nt in size, which are similar in sequence among family members and suppress protein translation through post-transcriptional mechanisms by matching predominately to the 3'-untranslated region (3'-UTR) of the target gene [1-4]. Computational estimations suggest that one third of protein-coding genes involving in embryogenesis, cell differentiation, metabolism and maturation are regulated by miRNAs [5, 6]. In addition, aberrant miRNA expression is reported to be associated with oncogenesis and tumor suppression [7-9]. Among many of the known miRNAs in cancer, recent studies verified that miR-30a is aberrantly expressed in a variety of carcinomas, including lung cancer, breast cancer, and osteosarcoma, which may serve as biomarkers for tumor prognosis [10, 11]. Thus, to develop a rapid and sensitive method for miRNAs identification and quantification in tumor cells is highly desirable in biomedical research, further may provide an applicable approach for the early diagnosis of cancer.

Currently available common miRNAs sensing techniques including Northern blot [12, 13], real-time quantitative PCR (RT-PCR) [14, 15] and microarrays [16, 17]. However, these strategies suffer from one or more of following disadvantages: relatively long analysis time, inadequate sensitivity and stability, higher costs. In an effort to resolve the aforementioned limitations of the above methods, some alternative detection methods such as hybridization-based biosensors have been developed, including rolling circle amplification (RCA) [18], molecular beacon [19] and isothermal exponential amplification [20]. Since DNA hybridization does not strictly obey Watson-Crick base pairing rules, a probe has the potential to hybridize with different oligonucleotides including various sites, thus may lead to false-positive results. Thus, DNA hybridization often needs optimization. Over a long time, various techniques to improve the specificity of nucleic acids hybridization were developed including molecular beacons [21], triple-stem clamp nanoswitches [22] and enhance the hybridization reaction temperature near melting temperature (T_m) [23]. However, most of these hybridization-based assays have restricted the power for the specific identification of single-base variants because of the small difference between a perfectly matched duplex and a duplex containing only one mismatched base. Furthermore, the complicated reaction condition of these methods limits their application in live cells. Weizmann and Kotov *et. al* utilizes cascade hybridization reaction and self-assembled nanomaterials to achieve ultrasensitive detection and quantification of miRNA in living cells [24, 25]. In consideration of unique characteristics of miRNA including small size, high sequence homology among family members, low abundance, and susceptibility to degradation, the improved profile strategy for real-time detection and visualization of miRNAs in live cells is urgently needed.

[a] *Key Laboratory of Laboratory Medical Diagnostics of Education, Department of Laboratory Medicine, Chongqing Medical University, Chongqing 400016, P. R. China.*
[b] *State Key Laboratory of Stem Cell and Reproductive Biology, Institute of Zoology, Chinese Academy of Sciences, Beijing 100101, P. R. China*
[c] *Department of Orthopaedics, Tianjin First Center Hospital, Tianjin 300192, P. R. China.*
* *Corresponding authors. E-mail address: qwzuo@qq.com or 17305105@qq.com*

View Article Online
DOI: 10.1039/C6RA05131F

Due to easy DNA loading, high surface to volume ratio, excellent biocompatibility, high intracellular stability and optical properties, gold nanoparticles (AuNPs) are widely used as probe carrier and quencher both *in vitro* and *in vivo* [26-28]. In this article, we presented a highly sensitive and selective method for the detection of miR-30a by coupling the gold nanoparticles (AuNPs) distance-dependent fluorescence quenching with thiolated double-chain structured probe based on improved strand displacement reaction [29](as shown in Scheme 1). The pre-formed protector/complement heteroduplex probe, which was labeled with a fluorophore (FAM, 6-carboxy-fluorescein) at the 5'-terminus of protector and a thiol (-SH) at the 3'-terminus of complement, was assembled on the AuNPs surface with about 20 nm in diameter via Au-S coordinate bond. The probe is non-fluorescent due to the close proximity of the fluorophore and quencher AuNPs. Only in the presence of accurately matched miR-30a target can the strand displacement reaction happen and produce fluorescent thus enable the high selectivity (details seen content 3.1 DNA sequence design). To monitor target miR-30a expression levels in live cells, AuNPs functionalizing thiolated pre-formed probe via gold-thiol bond packaged with Lipofectamine 2000 were incubated with intended cells. In the presence of target miR-30a, the protector strand was displaced and kept AuNP at a distance via strand displacement reaction. Finally the fluorescence in cells can be imaged using fluorescence microscopy to realize the detection of miR-30a in different cells.

<Scheme 1>

2. Materials and methods

2.1. Reagents and materials

All oligonucleotide sequences were synthesized by Shanghai Sangon Biotechnology Co. (Shanghai, China) and used without further purification; their sequences were listed in Table S1. Hydrogen tetrachloroaurate trihydrate ($HAuCl_4 \cdot 3H_2O$) were purchased from Shanghai Sangon Biotechnology (Shanghai, China). LipofectamineTM 2000 was obtained from Thermo Fisher Scientific (Waltham, USA) for cell transfection of AuNP-probe. DAPI (4', 6-diamidino-2-phenylindole) is a nuclear fluorescent stain obtained from Beyotime biotechnology. All other reagents were of analytical reagent grade without further purification before use. The water used throughout all experiments was purified through a Millipore system (>18.2M $\Omega \cdot cm^2$).

2.2 Fabrication of AuNP and AuNP-probe

AuNPs of approximately 20 nm in diameter were fabricated according to established procedures [30]. The prepared AuNP were functionalized with thiol double strand probe, according to the protocol described previously with slight modification [31]. Briefly, the AuNP solution was concentrated 2-fold by centrifugation. Equimolar protector and complement strand were heated at 50 °C and slowly cooled down to room temperature to form double-stranded probe. Then 10 μL of 100 μM pre-formed double-stranded probe was mixed with 1 mL concentrated AuNP and incubated at 4°C for 16 h under gentle stirring. Subsequently, 10 μL of 1% SDS was injected with shaking at room temperature for 1 h to stabilize AuNP. Then 100 μL of 1 M NaCl solution was added slowly and aged for 12 h. After that, excess probe were removed by centrifugation three times. At last, the precipitate was resuspended in 1 mL PBS (pH 7.4) for 1 h on a vortex stirrer for further use.

2.3 Instrumentation

UV–visible absorption spectroscopy (NANODROP1000 Spectrophotometer, Thermo, USA) and transmission electron microscopy (TEM, H600, Hitachi, Japan) were used to investigate the fabrication of AuNPs-probe. All fluorescence measurements were carried out on a Cary Eclipse fluorometer (Agilent, USA). Scan parameters: excitation wavelength, 480 nm; emission wavelength, 520nm; scan range: from 490 to 540 nm. Kinetics parameters: scan time, 60 min; scan intervals, 1 min; integration time, 6 sec; excitation wavelength, 480 nm; emission wavelength, 520 nm.

2.4 Cell culture and lipid nanoparticles transfection

Four kinds of different cell lines, 293T (human renal epithelial cell line with lower expression level of miR-30a), 143B (high malignant osteosarcoma cell line), MG63 (low malignant osteosarcoma cell line), iMEF (immortalized mouse embryonic fibroblast) were purchased from American Type Culture Collection (ATCC, Manassas, VA, USA) and maintained in Dulbecco's modified Eagle's medium (DMEM, Hyclone, USA) supplemented with 10% fetal bovine serum (FBS, Gibco, USA) and 100 U/ml streptomycin/penicillin at 37 °C in 5 % of CO_2. Lipofectamine 2000 is a cationic liposome formulation that functions by complexing with AuNP-probe, allowing them to overcome the electrostatic repulsion of the cell membrane and to be taken up by the cell. Cells cultured in 24-well plates were incubated with AuNP-probe by liposome package for 4 h, and then fluorescent images of the cells were obtained using a fluorescence microscopy equipped with a 20 objective (Olympus IX 71, Tokyo, Japan) and a CoolSNAPcf charge coupled device (CCD) camera (Photometrics, Tucson, AZ) with Metamorph image analysis software (Molecular Devices, Sunnyvale, CA) after extensive washing with PBS, all experimental were taken at least three independent measurements.

3. Results and discussion

3.1 DNA sequence design

For strand displacement reaction, the target can replace the protector strand from the pre-formed dsprobe and forming a new target/complement duplex. This exchange can be monitored by the changing of quenched fluorophore to fluorescent following target induced strand displacement reaction. The ideal dsprobe should meet the following requirement: first, sufficient base-pair matches to remain thermally stable in the absence of a target; second, dsprobe should possesses fewer base-pair matches than target/complement; third, the dsprobe must expose an active site to bind target (usually called initial toehold). In brief, target strand was first combined to initial toeholds of the pre-formed duplex,

View Article Online
DOI: 10.1039/C6RA05131F

followed a branch migration process that resembles a random walk that makes the releasing of protector strand and forming of new target/complement duplexes.

To obtain the best performance, mfold and Van't Hoff equation were used to calculate Gibbs energy change (ΔG_0) and equilibrium constant (K_{eq}) respectively, further simulated the hybridization yield and discrimination factor (DF) in theory (see Table S2). Strand displacement reaction can be simply regarded as

$$\mathrm{A} + \mathrm{B/C} \rightleftharpoons \mathrm{A/B} + \mathrm{C}$$

$$K_{eq} = \frac{[\mathrm{A/B}][\mathrm{C}]}{[\mathrm{A}][\mathrm{B/C}]}$$

Where A denotes target or mutate target, B represents complement strand and and C represents protector strand. Gibbs free energy change (ΔG_0) was calculated using mfold software online (http://unafold.rna.albany.edu/) written by Zuker et al (see Table S2). The calculated ΔG_0 for target and mutate target for strand displacement reaction are shown blow (the parameters are: temperature, 25 °C; strand concentration: 100 nM; all of the data were calculated obey minimum free energy rules).

For the above reactions in theroy, we started with $[\mathrm{A}_0] = c$, $[\mathrm{B/C}]_0 = c$, and $[\mathrm{A/B}] = [\mathrm{C}] = 0$. Define $x = [\mathrm{C}]_{\mathrm{eq}}$ to be the concentration of displacement reaction product [C] at equilibrium. The reaction yield is then $\lambda = \frac{x}{c}$,

$$K_{eq} = \frac{[\mathrm{A/B}][\mathrm{C}]}{[\mathrm{A}][\mathrm{B/C}]} = \frac{x^2}{(c-x)^2}$$

$$x = \frac{c\sqrt{K_{eq}}}{1+\sqrt{K_{eq}}}$$

$$\lambda = \frac{\sqrt{K_{eq}}}{1+\sqrt{K_{eq}}}$$

Using complementary sequence as target, ΔG_0= -1.06 kcal/mol, yielding K_{eq} = 6.03 and $\lambda = 0.71$. In theory, random sequence can't replace the protector strand from the pre-formed complement/protector due to ΔG>0. Target can replace protector strand from pre-formed duplex to some extent. However, mismatch, deletion or insertion target barely took strand displacement reaction into occur. All of the above ensured the specificity of the proposed strategy.

3.2 Characterization of AuNPs and AuNPs-probe

TEM and Uv/vis were used to characterize the fabrication of AuNP and AuNP-probe (see Figure S1). The concentration of AuNP (c) can be expressed as c = A450/ε450, where A450 represent the absorption at 450 nm for a standard path length of 1 cm, ε450 is 3.87E+08 $M^{-1}cm^{-1}$. The final concentration of AuNP was calculated to be 3.7 nmol. The amount of probe loading on the AuNPs surface was determined using a reported protocol [32]. Briefly, the fluorescence intensity was first converted into probe concentrations using a standard linear calibration curve that was generated by using known concentrations of the FAM labeled probe with an identical conditions. The average number of probe per particle was 153, which was calculated by dividing the measured probe concentration by the original AuNP concentration.

3.3 Optimization experimental conditions

To achieve optimal sensing performance, the assay conditions such as temperature, pH and hybridization time were further refined (see Figure S2). The optimal incubation temperature was set as 25 °C, agreeing with the simulated results. Further the optimal pH and hybridization time were set as 7.0 and 30 min, respectively.

3.4 Feasibility of the proposed strategy

As a proof of concept experiment, the feasibility of the proposed method for target detection has been demonstrated. As shown in Figure 1A, the complement/protector hybridization shows a strong characteristic fluorescence signal at 520 nm (curve a). After self-assembled on the AuNPs surface, the fluorescence signal was almost completely quenched by the AuNPs due to fluorescence resonance energy transfer (curve d). Upon addition of target miR-30a, strand displacement reaction occurs and forcing FAM to be away from the AuNPs surface thus enable the fluorescence signal intensity recovers about 60% (curve b), compared to curve a. However, for spurious target, fluorescence signal (curve c) changed little because mutate target could not displace protector strand. Kinetic results showed that displacement strand reaction progressed rapidly for target, because the fluorescence signal tended to stabilization after about 30 min, whereas spurious target showed no obvious change (Figure 1B).

<Figure 1>

3.5 Quantitative measurement of miR-30a concentration in buffer solution

The sensitivity of the proposed strategy for the detection of miR-30a was investigated by varying the miR-30a concentration, As shown in Figure 2A, the fluorescence intensities increased as a function of increasing concentration of miR-30a from 5 pM to 200 pM. The results shown in the inset of Figure 2B revealed a good linear correlation between signal intensities and the logarithm of target concentrations ranging from 5 pM to 200 pM, with lower detection limit of 2.4 pM (at S/N=3 rules). The regression equation could be expressed as RFU=34.23ln(C/pM)-45.69, where RFU is the fluorescence intensity and C is the concentration of miR-30a, with a correlation coefficient (R) of 0.99. For each concentration added, the measurement has been repeated for at least three times independently.

<Figure 2>

3.6 Selectivity of the proposed strategy

To show the selectivity of the proposed strategy, four kinds of target analogues were used with the same concentration including non-complementary, single-base variation (mismatch, deletion and insertion) oligonucleotides. As shown in Figure 3A, the probe only responded effectively to the complementary target sequence. With single-base variation and noncomplementary sequences, much smaller value was obtained. The high selectivity can be attributed only to the presence of the target where the strand displacement reaction occurred.

View Article Online
DOI: 10.1039/C6RA05131F

<Figure 3>

3.7 Imaging in live cells

After confirming that AuNP-probe can work as expected in solution, we next examined whether AuNPs functionalizing thiolated pre-formed probe can detect miR-30a in live cells. In this study, we chose miR-30a as the assay target because it is specifically highly expressed in MG63 osteosarcoma cell line and is identified as a biomarker for the prognosis of osteosarcoma and several other cancers, including non-small cell lung cancer (NSCLC), gastric cancer and hepatocellular carcinoma (HCC) [33]. We chose four kinds of different cell lines, 293T (human renal epithelial cell line with lower expression level of miR-30a), 143B (high malignant osteosarcoma cell line), MG63 (low malignant osteosarcoma cell line), iMEF (immortalized mouse embryonic fibroblast) as our detection objects. Briefly, cells cultured in 24-well plates were incubated with gold nanoparticles by liposome package for 4 h, and then fluorescent images of the cells were obtained by fluorescence microscopy after extensive washing with PBS. We also carried out CCK-8 assay to evaluate cytotoxicity of AuNPs and liposome. Treatment of AuNPs or liposome induced little reduction in the viability of MG63 and iMEF cells, which indicated that they are generally nontoxic (Figure S3). The fluorescence images of cells showed that the intracellularly delivered AuNP-probe induced the increase of fluorescence signal of FAM with different intensity in each cell line, which was due to the discrepant expression level of miR-30a in these four kinds of cell lines (Figure 4A). Consistent with other reports, high malignant 143B cells exhibited lower expression of miR-30a than low malignant MG63 cells and normal fibroblast cells. In addition, relative miR-30a expression levels were also confirmed by the end point analysis of qRT-PCR (Figure 4B). The data in Figure 4B also showed that results obtained from two methods are basically the same, indicating that the proposed assay method has a promise in practical application with great accuracy and reliability for miR-30a detection.

<Figure 4>

To analyze the time influence on the detection efficiency in live cells, MG63 cells expressing high levels of miR-30a were taken as example to explain the application of the method. The MG63 cells were first cultured in 24-well plates at a density of 2×105 cells per well and incubated with gold nanoparticles by liposome package for different time period (0, 0.5, 2, 4 and 8 h). At the end of each time point, cells were analyzed by fluorescence microscopy. The fluorescent images indicated that the fluorescence corresponding to FAM was visible at 0.5 h and reach to the strongest intensity at 4 h (Figure 5). The same phenomenon was observed in another kind of cell, iMEF (Figure S4).

<Figure 5>

4. Conclusion

In summary, the vital role of miRNA in cell regulation processes and its association with various human cancers as a tumor suppressor or an oncogenic factor indicate great demand for an accurate and rapid approach for highly efficient miRNA imaging in live cells. In this article, AuNP was used due to its great efficiency of quench fluorescence and also acted as a probe carrier to enter cells. Our proposed strategy has the ability to quantitative detection of miRNA with high specificity and sensitivity in homogeneous solutions; we further extended our strategy for the quantitative detection of miRNA expression levels in live cells with high precision and discrimination power. Compared with complicated RNA isolation step in Northern blot and PCR methods, our proposed strategy allowed to monitor mature miRNA expression levels in live cells by simple treatment of AuNPs/liposome complex to the cells without requiring any additional steps. Our method is more suitable for overexpressed miRNAs imaging and offers a programmable fluorescent that can be applied to monitor any miRNA target of interest in a live cell.

Acknowledgements

We thank Dr. Liwei Jia (Case Western Reserve University) for her kindly revising for this article. This study was supported by the National Natural Science Foundation of China (No. 81102035 and 31401270), and Science & Technology Fund of Tianjin Municipal Commission of Health and Family Planning (No. 2014KZ025).

Notes and references

1. S. S. Hébert and B. De Strooper, *Science*, 2007, **317**, 1179-1180.
2. L. He and G. J. Hannon, *Nature Reviews Genetics*, 2004, **5**, 522-531.
3. M. V. Joglekar, V. M. Joglekar and A. A. Hardikar, *Gene Expression Patterns*, 2009, **9**, 109-113.
4. H.-A. Rafiee-Pour, M. Behpour and M. Keshavarz, *Biosensors and Bioelectronics*, 2016, **77**, 202-207.
5. C. Sevignani, G. A. Calin, L. D. Siracusa and C. M. Croce, *Mammalian Genome*, 2006, **17**, 189-202.
6. F. L. Xie, S. Q. Huang, K. Guo, A. L. Xiang, Y. Y. Zhu, L. Nie and Z. M. Yang, *Febs Letters*, 2007, **581**, 1464-1474.
7. M. V. Iorio, M. Ferracin, C.-G. Liu, A. Veronese, R. Spizzo, S. Sabbioni, E. Magri, M. Pedriali, M. Fabbri and M. Campiglio, *Cancer research*, 2005, **65**, 7065-7070.
8. X. Wang, S. Tang, S.-Y. Le, R. Lu, J. S. Rader, C. Meyers and Z.-M. Zheng, *PloS one*, 2008, **3**, e2557.
9. A. Esquela-Kerscher and F. J. Slack, *Nature Reviews Cancer*, 2006, **6**, 259-269.
10. H. Zhu, H. Wu, X. Liu, B. Li, Y. Chen, X. Ren, C.-G. Liu and J.-M. Yang, *Autophagy*, 2009, **5**, 816-823.
11. G. Long, F. Wang, Q. Duan, S. Yang, F. Chen, W. Gong, X. Yang, Y. Wang, C. Chen and D. W. Wang, 2012.
12. M. Lagos-Quintana, R. Rauhut, W. Lendeckel and T. Tuschl, *Science*, 2001, **294**, 853-858.
13. A. Válóczi, C. Hornyik, N. Varga, J. Burgyán, S. Kauppinen and Z. Havelda, *Nucleic acids research*, 2004, **32**, e175-e175.
14. E. Varkonyi-Gasic, R. Wu, M. Wood, E. F. Walton and R. P. Hellens, *Plant methods*, 2007, **3**, 1-12.
15. N. Redshaw, T. Wilkes, A. Whale, S. Cowen, J. Huggett and C. A. Foy, *Biotechniques*, 2013, **54**, 155-164.

View Article Online
DOI: 10.1039/C6RA05131F

16. J. M. Lee and Y. Jung, *Angewandte Chemie International Edition*, 2011, **50**, 12487-12490.
17. J. M. Thomson, J. Parker, C. M. Perou and S. M. Hammond, *Nature methods*, 2004, **1**, 47-53.
18. Y. Cheng, X. Zhang, Z. Li, X. Jiao, Y. Wang and Y. Zhang, *Angewandte Chemie*, 2009, **121**, 3318-3322.
19. H. Yin, Y. Zhou, H. Zhang, X. Meng and S. Ai, *Biosensors and Bioelectronics*, 2012, **33**, 247-253.
20. R. Huang, Y. Liao, X. Zhou and D. Xing, *Analytica chimica acta*, 2015, **888**, 162-172.
21. S. Tyagi and F. R. Kramer, *Nature biotechnology*, 1996, **14**, 303-308.
22. Y. Xiao, X. Lou, T. Uzawa, K. J. Plakos, K. W. Plaxco and H. T. Soh, *Journal of the American Chemical Society*, 2009, **131**, 15311-15316.
23. A. H. Yang, K. Hsieh, A. S. Patterson, B. S. Ferguson, M. Eisenstein, K. W. Plaxco and H. T. Soh, *Angewandte Chemie*, 2014, **126**, 3227-3231.
24. Z. Cheglakov, T. M. Cronin, C. He and Y. Weizmann, *Journal of the American Chemical Society*, 2015, **137**, 6116-6119.
25. S. Li, L. Xu, W. Ma, X. Wu, M. Sun, H. Kuang, L. Wang, C. Xu and N. A. Kotov, *Journal of the American Chemical Soci*ety, 2015, **138,** 306–312.
26. H. Wei, B. Li, J. Li, E. Wang and S. Dong, *Chem. Commun.*, 2007, 3735-3737.
27. R. Elghanian, J. J. Storhoff, R. C. Mucic, R. L. Letsinger and C. A. Mirkin, *Science*, 1997, **277**, 1078-1081.
28. D. A. Giljohann, D. S. Seferos, P. C. Patel, J. E. Millstone, N. L. Rosi and C. A. Mirkin, *Nano letters*, 2007, **7**, 3818-3821.
29. Z. Zhang, J. long Li, J. Yao, T. Wang, D. Yin, Z. Chen and G. Xie, *Biosensors and Bioelectronics*, 2016, **79**, 488-494.
30. D. A. Giljohann, D. S. Seferos, W. L. Daniel, M. D. Massich, P. C. Patel and C. A. Mirkin, *Angewandte Chemie International Edition*, 2010, **49**, 3280-3294.
31. X. Fang, W. Jiang, X. Han and Y. Zhang, *Microchimica Acta*, 2013, **180**, 1271-1277.
32. L. Qiu, L. Qiu, Z.-S. Wu, G. Shen and R.-Q. Yu, *Analytical chemistry*, 2013, **85**, 8225-8231.
33. R. Zhang, S. Yan, J. Wang, F. Deng, Y. Guo, Y. Li, M. Fan, Q. Song, H. Liu and Y. Weng, *Tumour biology: the journal of the International Society for Oncodevelopmental Biology and Medicine*, 2015.

View Article Online
DOI: 10.1039/C6RA05131F

RSC Advances

COMMUNICATION

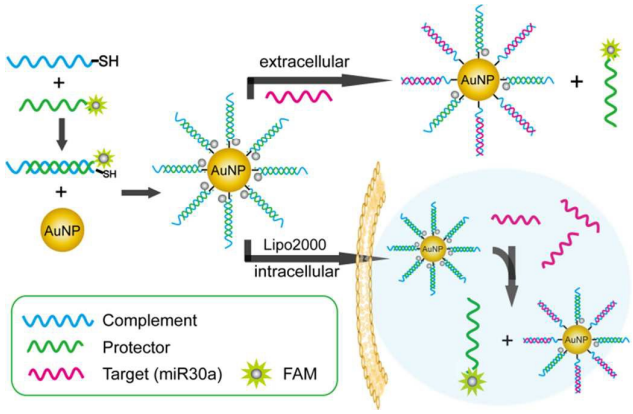

Scheme 1 Scheme illustration of the proposed miRNA sensor based on double-stranded probe modified AuNPs for sensitive and selective detection of microRNA 30a in solution and live cell.

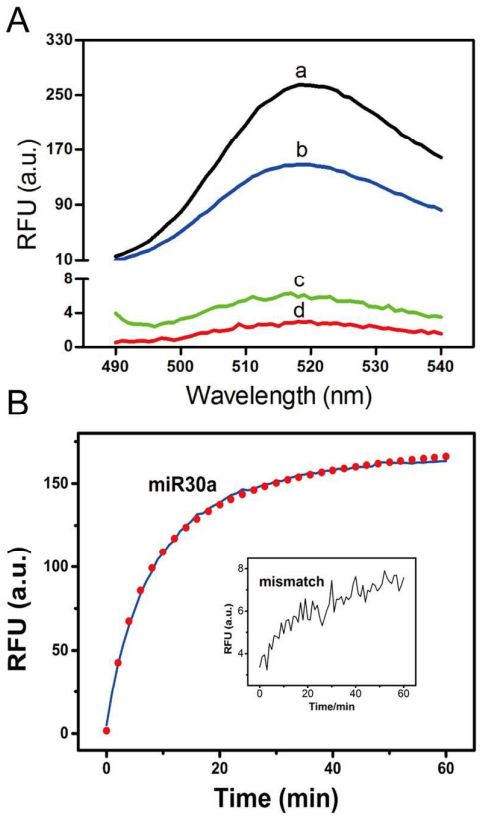

Figure 1 (A) Fluorescence emission spectra of the double strand probe in PBS (pH 7.4) before (curve a) and after (curve d) assembled on the AuNPs surface. Curve b and curve c shows fluorescence spectrum after hybridized with target miR-30a and spurious target. (B) Kinetic analysis of fluorescence intensity on the hybridization time for AuNP-probe incubated with miR-30a target and one mismatch target (shown inset). The dotted line shows simulated curves simulated according to a second order reaction rules.

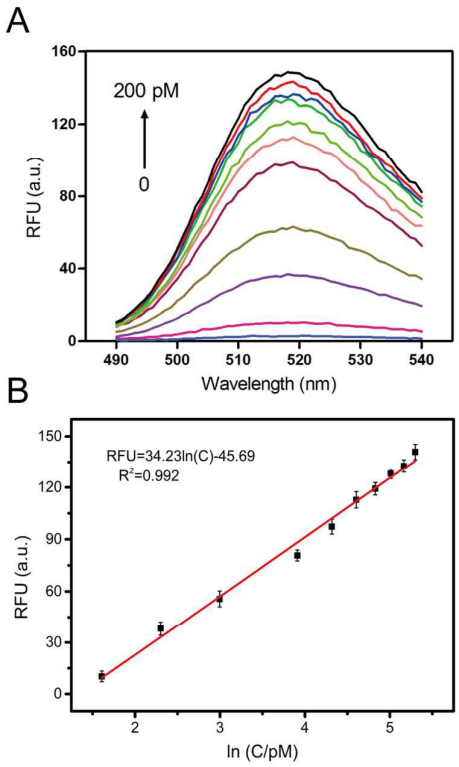

Figure 2 (A) Dependence of the fluorescence intensities on the concentrations of target miR-30a. From bottom to top, the concentration of target miRNA is 0, 5, 10, 20, 50, 75, 100, 125, 150, 175 and 200 pM, respectively. (B) A linear relationship between the fluorescence response and the logarithm of concentrations of miR-30a ranging from 5 to 200 pM . Error bars represent standard deviations of three measurements.

View Article Online
DOI: 10.1039/C6RA05131F

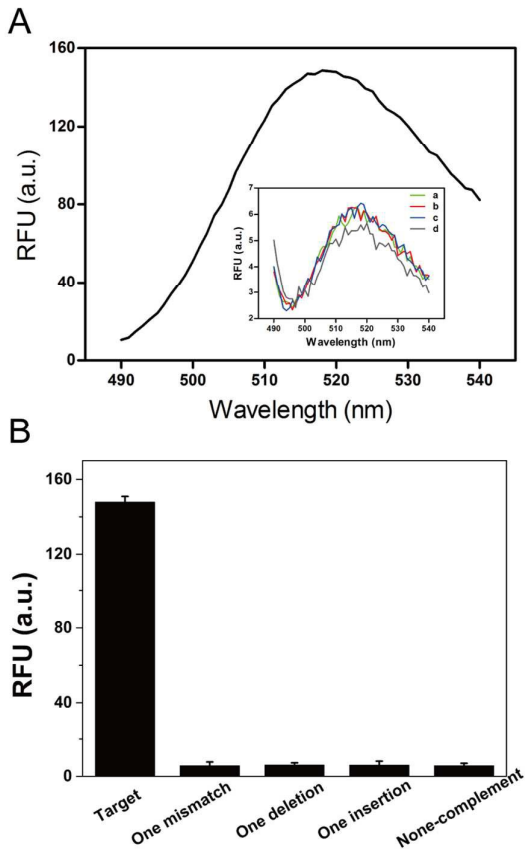

Figure 3 (A) Fluorescence spectra of AuNP-probe incubated with miRNA 30a and one mismatch (curve a), one deletion (curve b), one insertion (curve c), random sequence (curve d). (B) Selectivity tests of this assay. Error bars show the standard deviation of three experiments.

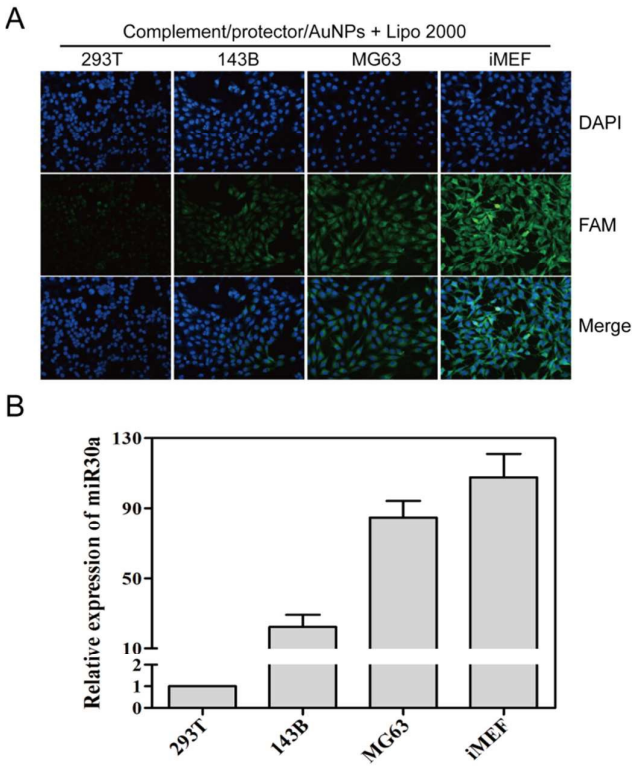

Figure 4 (A) Qualitative and quantitative detection of miR-30a in four cell lines (293T, 143B, MG63 and iMEF). Fluorescent images of the cells were taken after 4 h of treatment of AuNP-probe and lipofectamine 2000 to the cells, followed by extensive washing. The relative expression levels of miR-30a could be estimated from different degree of fluorescent intensities shown in the fluorescent images. (B) qRT-PCR was used for detecting the relative expression of miR30a in 4 kinds of cell lines.

View Article Online
DOI: 10.1039/C6RA05131F

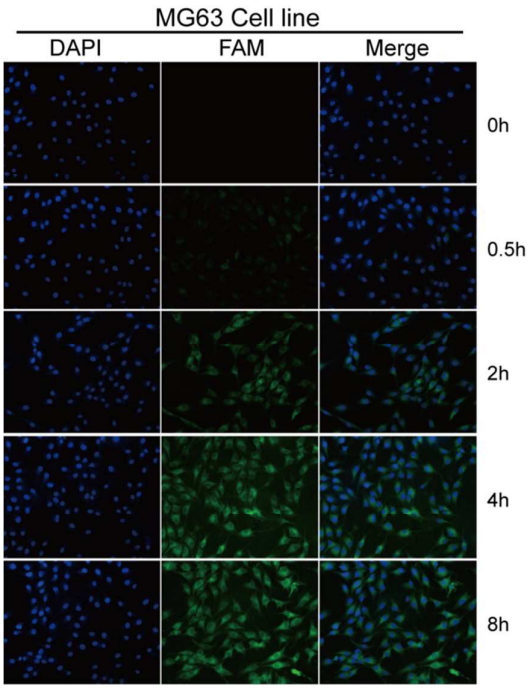

Figure 5 Fluorescence signals were visualized for MG63 cell line as incubation time increased from 0 to 8 h.

View Article Online
DOI: 10.1039/C6RA05131F

Graphical Abstract

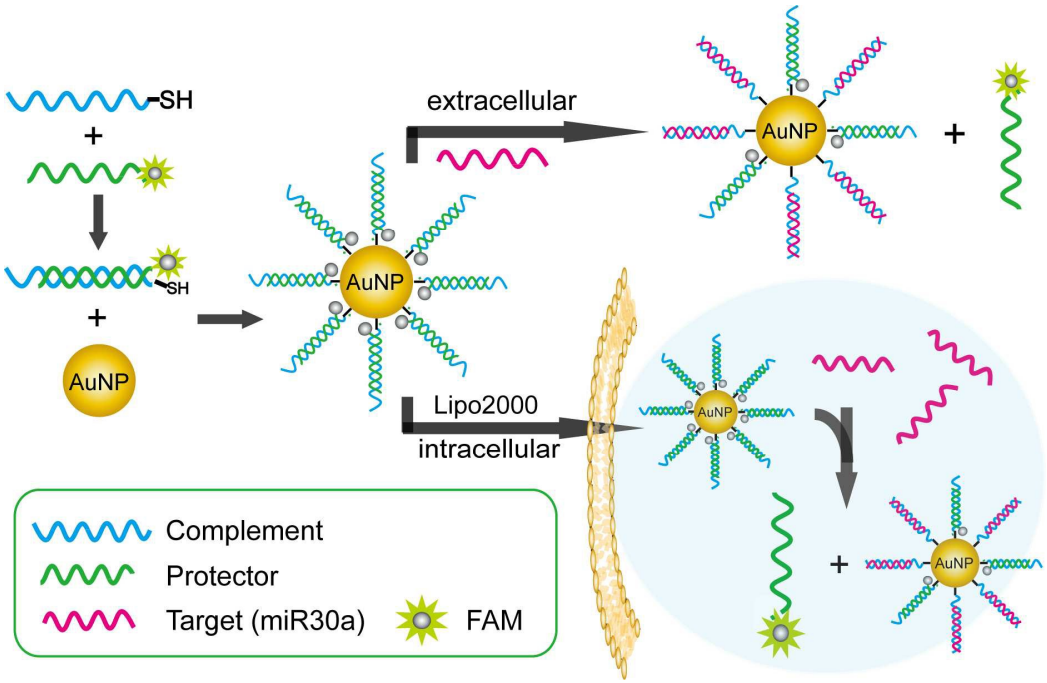

In this article, we reported a double-stranded DNA probe modified gold nanoparticle used as both "nano-flares" and transfection agents to quantify miR-30a in solution and visualize in live cells.